Exploring subluminous X-ray binaries

Degenaar, N.D.

Publication date
2010

2

Chandra and *Swift* observations of the quasi-persistent neutron star transient EXO 0748–676 back to quiescence

N. Degenaar, R. Wijnands, M.T. Wolff, P.S. Ray, K.S. Wood, J. Homan, W.H.G. Lewin, P.G. Jonker, E.M. Cackett, J.M. Miller and E.F. Brown

Monthly Notices of the Royal Astronomical Society, 2009, 396, L26

Abstract – The quasi-persistent neutron star X-ray transient and eclipsing binary EXO 0748–676 recently started the transition to quiescence following an accretion outburst that lasted more than 24 years. We report on two *Chandra* and twelve *Swift* observations performed within five months after the end of the outburst. The *Chandra* spectrum is composed of a soft, thermal component that fits to a neutron star atmosphere model with $kT^{\infty} \sim 0.12$ keV, joined by a hard powerlaw tail that contributes $\sim$ 20% of the total 0.5–10 keV unabsorbed flux. The combined *Chandra*/*Swift* data set reveals a relatively hot and luminous quiescent system with a temperature of $kT^{\infty} \sim 0.11 - 0.13$ keV and a bolometric thermal luminosity of $\sim 8.1 \times 10^{33} - 1.6 \times 10^{34}\ (\mathrm{D}/7.4\ \mathrm{kpc})^2$ erg s^{-1}. We discuss our results in the context of cooling neutron star models.

2.1 Introduction

Neutron star X-ray transients spend the vast majority of their time in quiescence, in which they are dim with typical luminosities of $\sim 10^{32-34}$ erg s^{-1}, but occasionally show an immense X-ray brightening in which their luminosity can rise to levels of $\sim 10^{36-38}$ erg s^{-1} (e.g., Chen et al. 1997). Their quiescent X-ray spectra are observed to consist of one or two components; a soft, thermal component ($kT \sim 0.1-0.2$ keV), and/or a hard powerlaw tail (dominating above 2 keV, photon index $\Gamma \sim 1-2$; e.g., Asai et al. 1996).

Several explanations have been put forward to describe the quiescent emission of neutron star transients, such as low-level accretion (e.g., Zampieri et al. 1995; Menou et al. 1999) or emission mechanisms connected to the magnetic field of the neutron star (see e.g., Campana 2003). However, the soft spectral component is most often interpreted as thermal emission emerging from the neutron star surface (Brown et al. 1998). During accretion outbursts, a series of nuclear reactions deposit heat in the neutron star crust (e.g., Haensel & Zdunik 1990a, 2008; Gupta et al. 2007), which spreads over the neutron star. The gained heat is radiated as thermal emission from the surface once the system returns to quiescence. In this interpretation the quiescent thermal emission depends on the time-averaged accretion rate of the system (e.g., Brown et al. 1998), as well as on the neutrino emission mechanism that operates in the core, which regulates the cooling (e.g., Yakovlev et al. 2003).

There exists a small group of quasi-persistent X-ray transients, which undergo prolonged accretion outbursts with a duration of years to decades rather than the usual weeks to months (e.g., Wijnands 2004). In these systems, the neutron star crust is substantially heated and becomes thermally decoupled from the core. Once the outburst ends, the crust will cool down primarily through heat conduction towards the core, until eventually thermal equilibrium is re-established (e.g., Rutledge et al. 2002b). This thermal relaxation depends strongly on the properties of the crust, such as the thermal conductivity.

In recent years, the quasi-persistent X-ray binaries KS 1731–260 and MXB 1659–29 have been monitored during the transition towards quiescence with *Chandra* and *XMM-Newton* following accretion outbursts with a duration of ~ 12.5 and ~ 2.5 yr, respectively (Wijnands et al. 2001, 2002a, 2003, 2004; Cackett et al. 2006, 2008a). For both systems, these observations revealed a lightcurve that decayed exponentially from a bolometric luminosity of $\sim (3-5)\times 10^{33}$ erg s^{-1} a few months after the outburst, levelling off to $\sim (2-5)\times 10^{32}$ erg s^{-1} several years later (Cackett et al. 2006, 2008a). Whereas the initial stages of this decaying curve are set by the properties of the crust, the quiescent base level reflects the thermal state of the core (e.g., Brown & Cumming 2009). Confronting the observed cooling curves with thermal evolution models suggests that the neutron stars in both KS 1731–260 (Shternin et al. 2007)

and MXB 1659–29 (Brown & Cumming 2009) have a highly conductive crust. This idea is supported by theoretical plasma simulations of Horowitz et al. (2007), who demonstrated that the accreted matter will arrange itself in a lattice structure with a high thermal conductivity.

2.1.1 EXO 0748–676

Recently, the quasi-persistent neutron star X-ray transient EXO 0748–676 also started the transition to quiescence. This low-mass X-ray binary was initially discovered with *EXOSAT* in 1985 February (Parmar et al. 1986), although it appears as an *EXOSAT* slew survey source several times before this date (Reynolds et al. 1999, the earliest detection dates back to 1984 July 15). Prior to its discovery, EXO 0748–676 was serendipitously observed with *Einstein* in 1980 May, from which Garcia & Callanan (1999) deduced a kT ~0.2 keV blackbody source spectrum with a 0.5–10 keV luminosity of $\sim 5 \times 10^{33}\ (\mathrm{D}/7.4\ \mathrm{kpc})^2$ erg s^{-1}. The system displays X-ray dips and exhibits eclipses with a duration of ~ 8.3 min every 3.82 h (Parmar et al. 1986).

Ever since its discovery, EXO 0748–676 was consistently detected with luminosities $\gtrsim 10^{36}$ erg s^{-1} by various satellites. In particular, regular monitoring with *RXTE* showed that the source maintained a relatively steady 2–20 keV flux of approximately 2×10^{-10} erg cm^{-2} s^{-1}, since 1996 ($L_{\mathrm{X}} \sim 1 \times 10^{36}\ (\mathrm{D}/7.4\ \mathrm{kpc})^2$ erg s^{-1}; Wolff et al. 2008a). However, observations with the Proportional Counter Array (PCA) obtained on 2008 August 12 signalled a decrease in 2–20 keV source flux, down to $\sim 7 \times 10^{-11}$ erg cm^{-2} s^{-1} ($L_{\mathrm{X}} \sim 5 \times 10^{35}\ (\mathrm{D}/7.4\ \mathrm{kpc})^2$ erg s^{-1}; Wolff et al. 2008a). This decline was confirmed when *Swift* observations with the X-ray Telescope (XRT) performed on 2008 September 28 found the source at a 0.5–10 keV flux of $\sim 2 \times 10^{-12}$ erg cm^{-2} s^{-1} ($L_{\mathrm{X}} \sim 1 \times 10^{34}\ (\mathrm{D}/7.4\ \mathrm{kpc})^2$ erg s^{-1}; see Section 2.2.2). Subsequent *RXTE*/PCA observations, carried out on 2008 October 5, failed to detect EXO 0748–676 (Wolff et al. 2008b), consistent with the flux level observed with *Swift*/XRT. Optical and near-IR observations of the optical counterpart of EXO 0748–676 (UY Vol), performed in October 2008, detected a decrease in its optical brightness compared with the active X-ray state (Hynes & Jones 2008; Torres et al. 2008).

The observed large decline in X-ray and optical luminosity suggest that EXO 0748–676 is returning to quiescence after having actively accreted for 24 yrs. With its long outburst duration, EXO 0748–676 is a good candidate to look for thermal relaxation of the accretion heated neutron star crust now that the system is returning to quiescence. In this Letter we report on *Chandra* and *Swift* observations of EXO 0748–676 performed within the first five months after the accretion outburst ceased.

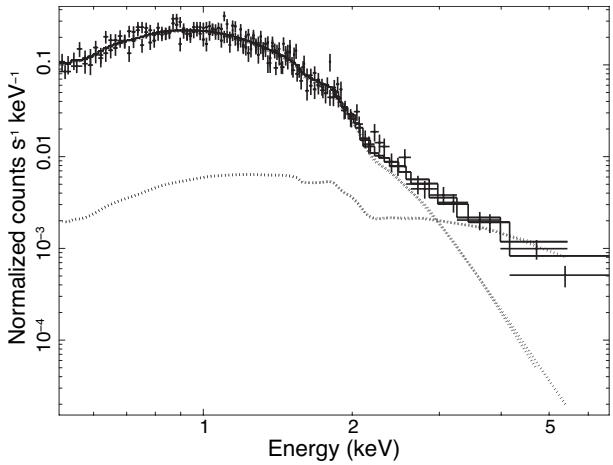

Figure 2.1: Spectra of both *Chandra* observations, along with the model fit (solid line) for $D = 7.4$ kpc, $\Gamma = 1$ and $M = 1.4$ $M_\odot$. The dotted lines indicate the NSATMOS and powerlaw components.

2.2 Observations, analysis and results

2.2.1 Chandra data

As part of our *Chandra* Target of Opportunity (TOO) proposal EXO 0748–676 was observed with *Chandra*/ACIS-S on 2008 October 12–13 22:09–02:51 UTC (obs ID 9070) and on 2008 October 15 12:46–17:13 UTC (obs ID 10783), for on-source times of 13.8 and 13.3 ks, respectively. We used the CIAO tools (v. 4.0) and standard *Chandra* analysis threads to reduce the data. No background flares were found, so all data were used for further analysis. The ACIS-S3 CCD was operated in a 1/8 sub-array to circumvent any possible pile-up problems. For the resulting frame-time of 0.4 s and the observed fluxes (see Table 2.1), the pile-up fraction was $< 4\%$.

Source spectra and lightcurves were extracted from a circular region with a radius of $3''$ centred on the position of EXO 0748–676. Background events were obtained from an annular region with an inner (outer) radius of $10''$ ($25''$). The lightcurves of both *Chandra* observations display one eclipse at times consistent with the ephemeris of Wolff et al. (2009). During the eclipses, only one photon was detected from the source region and a similar amount was found for the normalized background. This indicates that X-rays from the neutron star are not detected during the eclipses. To calculate the correct non-eclipse time-averaged fluxes, we reduced the exposure times of the fits files by 500 s (the approximate duration of the eclipses; Parmar et al. 1986;

Table 2.1: Results from fitting the *Chandra*/ACIS-S spectral data.

		$\Gamma = 1$		
Parameter	5.0 kpc	5.0 kpc	7.4 kpc	8.3 kpc
$N_{\rm H}$ $(10^{22}$ cm$^{-2})$	0.12 ± 0.03	0.12 ± 0.02	0.12 ± 0.02	0.12 ± 0.03
$kT_{\rm eff}^{\infty}$ (eV)	112 ± 14	113 ± 12	118 ± 4	119 ± 4
$M_{\rm NS}$ $(M_{\odot})$	(1.4)	1.8 ± 0.4	(1.4)	(1.4)
$R_{\rm NS}$ (km)	11.9 ± 2.8	(10)	17.1 ± 3.2	18.8 ± 3.4
$F_{\rm X}$ (0.5–10 keV)	1.3 ± 0.1	1.3 ± 0.1	1.3 ± 0.2	1.3 ± 0.1
$F_{\rm X}^{\rm th}$ (0.01–100 keV)	1.5 ± 0.2	1.5 ± 0.2	1.5 ± 0.1	1.5 ± 0.2
$L_{\rm X}$ (0.01–100 keV)	4.5 ± 0.6	4.5 ± 0.5	9.8 ± 1.0	10.2 ± 1.2
		$\Gamma = 2$		
Parameter	5.0 kpc	5.0 kpc	7.4 kpc	8.3 kpc
$N_{\rm H}$ $(10^{22}$ cm$^{-2})$	0.14 ± 0.03	0.14 ± 0.03	0.14 ± 0.03	0.14 ± 0.03
$kT_{\rm eff}^{\infty}$ (eV)	106 ± 9	108 ± 12	112 ± 8	114 ± 8
$M_{\rm NS}$ $(M_{\odot})$	(1.4)	2.0 ± 0.3	(1.4)	(1.4)
$R_{\rm NS}$ (km)	14.0 ± 3.4	(10)	19.4 ± 4.1	21.3 ± 4.5
$F_{\rm X}$ (0.5–10 keV)	1.4 ± 0.1	1.3 ± 0.2	1.3 ± 0.1	1.3 ± 0.1
$F_{\rm bol}^{\rm th}$ (0.01–100 keV)	1.5 ± 0.2	1.5 ± 0.2	1.5 ± 0.2	1.5 ± 0.2
$L_{\rm bol}$ (0.01–100 keV)	4.5 ± 0.6	4.5 ± 0.5	9.8 ± 1.3	10.2 ± 1.6

Note. – The quoted errors represent 90% confidence levels and $\chi^2_{\nu} = 1.1$ for all fits (173 d.o.f.). $F_{\rm X}$ represents the total unabsorbed 0.5–10 keV flux, while $F_{\rm bol}^{\rm th}$ gives the bolometric NSATMOS flux (both in units of 10^{-12} erg cm^{-2} s^{-1}). $L_{\rm bol}$ is the bolometric luminosity (for the model distance) of the NSATMOS component in units of 10^{33} erg s^{-1}.

Wolff et al. 2009). Using the tool GRPPHA we binned the spectra to contain a minimum of 20 photons per bin.

The resulting spectra were fitted using XSPEC (v. 12.0; Arnaud 1996). The *Chandra* observations were performed < 3 days apart, and we did not find any significant spectral changes between the two when fitting the data sets separately. Therefore, we tied all spectral parameters between the two observations. We fitted the data with a neutron star atmosphere model NSATMOS (Heinke et al. 2006). The normalization of this model was always fixed to one, which corresponds to the entire neutron star surface emitting. Using only the NSATMOS model, the data above $\sim 2-3$ keV cannot be fit properly. If we add a powerlaw component, this improves a fit with the neutron star mass and radius fixed at $M_{\rm NS} = 1.4$ M$_{\odot}$ and $R_{\rm NS} = 10$ km from $\chi^2 = 217.7/174$ d.o.f. to $\chi^2 = 181.0/172$ d.o.f. (an F-test suggests a 1.3×10^{-7} probability of achieving this level of improvement by chance). The NSATMOS model calculates the effective temperature in the neutron star frame. We

converted this to the effective temperature as seen by an observer at infinity according to $kT_{\rm eff}^{\infty} = kT_{\rm eff}/(1+z)$, where $1+z = (1-R_{\rm s}/R_{\rm NS})^{-1/2}$ is the gravitational redshift factor, with $R_{\rm s} = 2GM_{\rm NS}/c^2$ being the Schwarzschild radius, G the gravitational constant and c the speed of light.

When the neutron star mass and radius are fixed to canonical values of $M_{\rm NS} = 1.4$ M$_\odot$ and $R_{\rm NS} = 10$ km, the best-fit yields $D = 3.4^{+1.4}_{-0.7}$ kpc, $\Gamma = 2.3 \pm 0.9$, $N_{\rm H} = (0.16 \pm 0.1) \times 10^{22}$ cm^{-2} and $kT_{\rm eff}^{\infty} = 100^{+14}_{-23}$ eV. The fitted distance is lower than the best estimate of 7.4 kpc (with an allowed range of 5–8.3 kpc), which was inferred from analysis of type-I X-ray bursts (Galloway et al. 2008a, but see Galloway et al. 2008b for possible additional uncertainties). If we keep the mass and radius at canonical values and in addition fix the distance to either $D = 7.4$ kpc or $D = 8.3$ kpc, we obtain $\Gamma < 0$. However, for $D = 5$ kpc we obtain $\Gamma = 0.7^{+1.6}_{-0.7}$, $N_{\rm H} = (0.10 \pm 0.01) \times 10^{22}$ cm^{-2} and $kT_{\rm eff}^{\infty} = 118 \pm 2$ eV.

Finally, we explored fits with the distance fixed at 5, 7.4 or 8.3 kpc, but with either the mass or the radius left to vary freely (and the other kept at its canonical value). Since the powerlaw slope is not well constrained, this parameter was fixed to $\Gamma = 1$ or $\Gamma = 2$. The free parameters for each fit are then the hydrogen column density ($N_{\rm H}$), the effective temperature ($kT_{\rm eff}$), the normalization of the powerlaw component and either the mass ($M_{\rm NS}$) or radius ($R_{\rm NS}$).

We deduced unabsorbed fluxes in the 0.5–10 keV energy band and calculated the bolometric flux of the thermal component by extrapolating the NSATMOS model (using a zero normalization for the powerlaw) for the energy range 0.01–100 keV. The powerlaw contribution to the total 0.5–10 keV unabsorbed flux is $\sim 16-17\%$ for the fits with $\Gamma = 1$ and $\sim 19-20\%$ if $\Gamma = 2$. The results are summarised in Table 2.1. For $D = 7.4$ kpc and $D = 8.3$ kpc the fits with the radius fixed at $R_{\rm NS} = 10$ km resulted in neutron star masses of $M_{\rm NS} > 2.5$ M$_\odot$, i.e., exceeding the causality limit of 2.23 M$_\odot$ for a neutron star radius of 10 km; these fits are not listed in Table 2.1. The spectra of both *Chandra* observations are plotted in Figure 2.1.

2.2.2 Swift data

In addition to the *Chandra* data, we obtained *Swift*/XRT TOO observations of EXO 0748–676 returning to quiescence (see Table 2.2 for an overview). The XRT data, collected in the photon counting (PC) mode, were processed using standard *Swift* analysis threads. We extracted source spectra (using XSELECT v. 2.3) from a circular region with a radius of 15″, while background spectra were obtained from an annular region with an inner (outer) radius of 50″ (100″). The spectra were grouped to contain bins with a minimum number of 10 photons. We reduced the exposure times of those observations that contained eclipses according to the ephemeris of Wolff et al. (2009) to calculate the correct non-eclipse time-averaged fluxes (see Table 2.2).

Table 2.2: Results from fitting the *Swift*/XRT spectral data.

Obs ID	Date	$t_{\rm exp}$ (ks)	$kT_{\rm eff}^{\infty}$ (eV)	$F_{\rm X}$	$F_{\rm bol}^{\rm th}$	$L_{\rm bol}$	χ^2_ν (d.o.f.)
51300025	2008-09-28	0.93	133 ± 9	2.3 ± 0.6	2.4 ± 0.7	16 ± 5	1.7 (2)
31272001*	2008-10-07	1.49	128 ± 11	1.9 ± 0.6	2.0 ± 0.7	12 ± 4	0.1 (2)
31272003/4*	2008-10-29/30	5.01	119 ± 5	1.4 ± 0.2	1.5 ± 0.2	9.4 ± 2	1.4 (10)
31272005*	2008-11-02	4.78	115 ± 5	1.1 ± 0.2	1.3 ± 0.2	8.3 ± 1	1.4 (10)
31272007	2008-11-28	3.04	121 ± 6	1.5 ± 0.3	1.6 ± 0.3	11 ± 2	1.0 (5)
31272008*	2008-12-05	3.40	122 ± 6	1.6 ± 0.3	1.7 ± 0.3	11 ± 2	0.8 (6)
31272009	2008-12-20	4.22	115 ± 5	1.2 ± 0.2	1.3 ± 0.3	8.8 ± 1	1.9 (9)
31272012	2009-01-10	3.71	118 ± 5	1.3 ± 0.2	1.5 ± 0.3	9.5 ± 2	1.1 (7)
31272013	2009-01-16	4.16	116 ± 5	1.3 ± 0.2	1.4 ± 0.2	9.2 ± 2	1.2 (8)
31272014	2009-01-23	1.45	113 ± 10	1.1 ± 0.4	1.2 ± 0.4	8.1 ± 3	0.1 (1)
31272015*	2009-01-30	3.95	116 ± 5	1.2 ± 0.2	1.4 ± 0.2	9.0 ± 1	0.8 (8)

Note. – The quoted errors represent 90% confidence levels. $F_{\rm X}$ represents the 0.5–10 keV total model flux (described in the text) and $F_{\rm bol}^{\rm th}$ gives the 0.01–100 keV NSATMOS flux. Both are given in units of 10^{-12} erg cm^{-2} s^{-1}. $L_{\rm bol}$ gives the 0.01–100 keV luminosity of the NSATMOS model component in units of 10^{33} erg s^{-1} and assuming a source distance of 7.4 kpc. The exposure times of observations marked with an asterisk were corrected for (parts of) eclipses.

We fitted all grouped *Swift* spectra with a combined NSATMOS and powerlaw model, were we fixed all parameters except the effective temperature. Different fits to the *Chandra* spectral data yield similar χ^2 values, so there is no preferential model to use for the *Swift* data (see Table 2.1). We picked the fit with $D = 7.4$ kpc (the best distance estimate), $\Gamma = 1$, $M_{\rm NS} = 1.4\,{\rm M}_{\odot}$, $R_{\rm NS} = 17.1$ km and $N_{\rm H} = 0.12 \times 10^{22}$ cm^{-2}. The powerlaw normalization was adjusted for each observation so that this component contributes 17% of the total 0.5–10 keV flux. To improve the statistics, we tied the spectral parameters between observations 31272003 and 31272004, which were performed only one day apart. The results are presented in Table 2.2.

Figure 2.2 displays the effective temperatures and thermal bolometric fluxes derived from the *Chandra* and *Swift* data. The *Chandra* observations (obtained < 3 days apart) are plotted as a single data point (with an error on the time to indicate the spread of the two observations). The *Swift* observations 31272003 and 31272004 are also plotted as a single point. The bottom panel displays the evolution of the effective temperature of EXO 0748–676together with the data points and curve fits of KS 1731–260 and MXB 1659–29 (taken from Cackett et al. 2006, 2008a). Cackett et al. (2006) set the reference time, t_0, for KS 1731–260 and MXB 1659–29 to the day of the last detection with *RXTE*/PCA. For EXO 0748–676 we set t_0 at 2008 September 5, which is in between the last detection with *RXTE*/PCA (August 12) and the first *Swift* observation (September 28).

2.3 Discussion

We obtained two *Chandra* and twelve *Swift* observations within five months after the cessation of the very long (~24 yrs) active period of EXO 0748–676. We found (assuming a neutron star atmosphere model NSATMOS) a relatively hot and luminous quiescent system with a temperature of $kT_{\rm eff}^{\infty} \sim 0.11 - 0.13$ keV and a thermal bolometric luminosity of $\sim (8.1 - 16) \times 10^{33}$ $({\rm D}/7.4\ {\rm kpc})^2$ erg s^{-1}. In addition to a soft, thermal component, the *Chandra* data reveal a hard powerlaw tail, which contributes $\sim 20\%$ to the total 0.5–10 keV luminosity of 8.5×10^{33} $({\rm D}/7.4\ {\rm kpc})^2$ erg s^{-1}.

Comparing the evolution of the effective temperature of EXO 0748–676 with that of KS 1731–260 and MXB 1659–29 (bottom panel Figure 2.2) illustrates that the current data of EXO 0748–676 is consistent with the fit through the data of MXB 1659–29 (as well as with KS 1731–260 if the temperatures would be scaled). This suggests that the neutron star crust may thermally relax in the coming years, revealing a cooling curve as has been observed for KS 1731–260 and MXB 1659–29. The current data set can then provide an unique insight into the early stages of neutron star cooling, and can possibly put constraints on the amount of heating in the outer crustal layers (Brown & Cumming 2009).

However, the top and middle panel of Figure 2.2 suggest that the effective temperature and thermal bolometric flux of EXO 0748–676 have not decreased during the past three months (see also Table 2.2). The 0.5–10 keV luminosity remains approximately constant at $L_{\rm X} \sim 8 \times 10^{33}$ $({\rm D}/7.4\ {\rm kpc})^2$ erg s^{-1}, which is close to the value deduced from an *Einstein* observation in 1980 (see Section 2.1.1). There are several explanations that can account for the current high luminosity of EXO 0748–676 and are consistent with the *Einstein* detection of EXO 0748–676 in 1980.

Firstly, we cannot exclude the possibility that we detect low-level accretion from EXO 0748–676, since the resulting radiation spectrum may have a shape similar to that expected from crustal heating (e.g., Zampieri et al. 1995). We made Fast Fourier Transforms of the *Chandra* data (excluding the eclipses), but did not find any variability on short time scales ($< 10^4$ s) that might indicate continued accretion (Rutledge et al. 2002a).

If the observed thermal emission is due to crustal heating, then the constant luminosity might imply that the crust and core have already reached thermal equilibrium. The neutron star in EXO 0748–676 would then be relatively hot compared to other quiescent systems (see e.g., figure 4 of Heinke et al. 2009b). Such a high quiescent luminosity can be explained by standard core cooling. Since enhanced neutrino emission mechanisms are suppressed only when the density in the core is relatively low, this scenario would imply that the neutron star in EXO 0748–676 is not very massive and has not had enough time to accrete a significant amount of matter (the exact mass limit for enabling enhanced core cooling mechanisms is model dependent).

A high time-averaged mass-accretion rate can also give rise to a high quiescent luminosity. Parmar et al. (1986) stated that between 1970 and 1980 no outburst reaching $\sim 10^{36}$ erg s^{-1} was observed for EXO 0748–676 using *Uhuru, Ariel V* and *HEAO-1*, indicating that in the 10 yrs prior to the *Einstein* detection the source was in quiescence (at least, no similar long outburst as the most recent one occurred; shorter outbursts of weeks or even months cannot be excluded). Besides this, we cannot put any additional constraints on the duty cycle of EXO 0748–676. Normally, X-ray transients reside significantly longer in quiescence than in outburst, but for EXO 0748–676 the quiescence state might be similar in duration to the outburst episodes. The neutron star core temperature could then be maintained by repeated accretion episodes at a significantly higher level than would be the case if it would spend most of its time in quiescence.

Furthermore, a high quiescent luminosity can be accounted for if the neutron star crust has a low thermal conductivity, so that it will cool on a time scale of decades rather than a few years and remains hot for a long time (Rutledge et al. 2002b; Shternin et al. 2007). A drawback of this explanation is that there is no obvious reason why the neutron star in EXO 0748–676 would be so different in this respect from KS 1731–260 and MXB 1659–29, for which a low crust conductivity can be ruled out (Shternin et al. 2007; Brown & Cumming 2009). This would also oppose independent molecular dynamics simulations that predict a regular crystal lattice structure (Horowitz et al. 2007).

More *Chandra* observations of EXO 0748–676 are scheduled for this year and these will provide insight into the different scenarios discussed above.

Acknowledgments
We are grateful to the referee, Nathalie Webb, for very useful comments. This work was supported by NWO, the Netherlands Organization for Scientific Research. We acknowledge the use of the *Swift* public data archive. EMC was supported by NASA through the Chandra Fellowship Program. MTW, PSR and KSW acknowledge the United States Office of Naval Research. J.H. and W.H.G.L. gratefully acknowledge support from Chandra grant GO8-9045X.

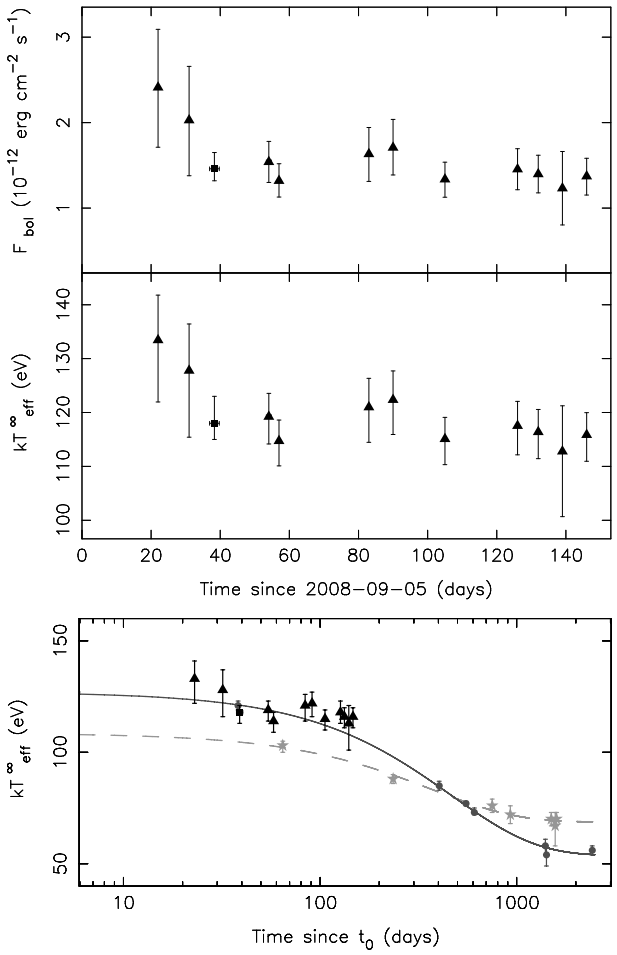

Figure 2.2: Evolution of the bolometric flux (top) and effective temperature (middle/bottom) of EXO 0748–676, deduced from *Chandra*/ACIS-S (squares) and *Swift*/XRT (triangles) observations. The bottom panel displays the effective temperatures of KS 1731–260 (light grey stars; from Cackett et al. 2006) and MXB 1659–29 (dark grey bullets; from Cackett et al. 2006, 2008a), in addition to the data points of EXO 0748–676. The exponential decay fits to the data of KS 1731–260 and MXB 1659–29 are also shown (dashed and solid line, respectively).